A non-canonical di-acidic signal at the C-terminus of Kv1.3 determines anterograde trafficking and surface expression

Ramón Martínez-Mármol[1], Mireia Pérez-Verdaguer[1], Sara R. Roig[1], Albert Vallejo-Gracia[1], Pelagia Gotsi[1], Antonio Serrano-Albarrás[1], María Isabel Bahamonde[2], Antonio Ferrer-Montiel[3], Gregorio Fernández-Ballester[3], Núria Comes[1] and Antonio Felipe[1,*]

[1]Molecular Physiology Laboratory, Departament de Bioquímica i Biologia Molecular, Institut de Biomedicina (IBUB), Universitat de Barcelona, Av. Diagonal 643, E-08028 Barcelona, Spain
[2]Institute for Bioengineering of Catalonia (IBEC), Feixa Llarga s/n, 08907 L' Hospitalet de Llobregat, Barcelona, Spain
[3]Instituto de Biología Molecular y Celular, Universidad Miguel Hernández, Av. de la Universidad s/n, 03202 Elche, Alicante, Spain
*Author for correspondence (afelipe@ub.edu)

Summary

Impairment of Kv1.3 expression at the cell membrane in leukocytes and sensory neuron contributes to the pathophysiology of autoimmune diseases and sensory syndromes. Molecular mechanisms underlying Kv1.3 channel trafficking to the plasma membrane remain elusive. We report a novel non-canonical di-acidic signal (E483/484) at the C-terminus of Kv1.3 essential for anterograde transport and surface expression. Notably, homologous motifs are conserved in neuronal Kv1 and Shaker channels. Biochemical analysis revealed interactions with the Sec24 subunit of the coat protein complex II. Disruption of this complex retains the channel at the endoplasmic reticulum. A molecular model of the Kv1.3–Sec24a complex suggests salt-bridges between the di-acidic E483/484 motif in Kv1.3 and the di-basic R750/752 sequence in Sec24. These findings identify a previously unrecognized motif of Kv channels essential for their expression on the cell surface. Our results contribute to our understanding of how Kv1 channels target to the cell membrane, and provide new therapeutic strategies for the treatment of pathological conditions.

Key words: Forward-traffic motifs, Lymphocytes, Neurons, Plasma membrane, Voltage-dependent K$^+$ channels

Introduction

Voltage-dependent potassium channels (Kv) control the resting membrane potential in mammalian cells (Hille, 2001). In this context, the Kv1.3 channel participates in the activity of sensory neurons and also controls the activation and proliferation of leukocytes (Vicente et al., 2003; Rivera et al., 2005; Cahalan and Chandy, 2009; Cavallin et al., 2010; Gazula et al., 2010). Therefore, Kv1.3 is considered to be a fundamental pharmacological target for diseases related to the nervous and immune systems (Koeberle and Schlichter, 2010; Villalonga et al., 2010; Conforti, 2012).

Kv1.3 signaling relies on the number of channels at the cell surface. Unlike other leukocytic channels, such as Kv1.5, Kv1.3 is very dynamic and is highly expressed on the cell surface, similar to the neuronal Kv1.4 (Manganas and Trimmer, 2000; Vicente et al., 2008). Many studies address the specific signatures responsible for the intracellular retention and membrane targeting of ion channels (Misonou and Trimmer, 2004). C-terminal sequences are essential for the expression of functional Kv channels. Human diseases such as juvenile epilepsy, Jervell and Lange-Nielsen syndrome, Romano–Ward syndrome and episodic ataxia are associated with mutations in the C-terminus of Kv7.2, Kv7.1, Kv11.1 and Kv1.1, respectively (Curran et al., 1995; Neyroud et al., 1997; Biervert et al., 1998; Manganas et al., 2001a; Rea et al., 2002). Therefore, the molecular determinants

responsible for the intracellular retention and surface expression of Kv channels are of considerable importance.

The surface expression is determined by the balance between ERR (endoplasmic reticulum retention) and FT (forward trafficking) signals (Misonou and Trimmer, 2004). RxR (x being any amino acid) signatures and similar highly positively charged motifs are very powerful ERR elements. In contrast, a VxxSL sequence is an efficient FT motif for the expression of Kv channels at the cell membrane (Misonou and Trimmer, 2004; Zhu et al., 2003). Analysis of Kv1.3 revealed that neither ERR nor FT canonical signatures are present in the protein. Therefore, the molecular determinants and the mechanisms responsible for Kv1.3 cell surface targeting remain largely unknown. Because deficient Kv1.3 expression has been associated with several autoimmune diseases and an irregular sensory physiology (Rivera et al., 2005; Nicolaou et al., 2007; Marks et al., 2009), the identification of these signatures is essential.

In the present study, we aimed to characterize the molecular determinants and cellular machinery responsible for Kv1.3 cell surface targeting. We have identified a Y^{479}MVIEE^{484} cluster at the C-terminus of the channel that was responsible for efficient Kv1.3 forward trafficking. This domain is highly conserved in neuronal isoforms of the Kv1 family. The di-acidic (E483/484) motif within the Y^{479}MVIEE^{484} cluster was the main determinant for Kv1.3 surface expression. This motif interacts with the coat

protein complex II (COPII) to trigger ER-to-Golgi anterograde transport to the plasma membrane. This study identifies a novel signal in Kv channels that contributes to our understanding of the mechanisms underlying ion channel trafficking and the ability of cells to fine-tune cellular responses.

Results

The C-terminal domain is necessary for effective Kv1.3 membrane surface targeting

The location of Kv1.3 has important consequences for cellular physiology (Panyi et al., 2004; Rivera et al., 2005). Unlike Kv1.5, Kv1.3 efficiently targets to membranes (Vicente et al., 2008). Kv1.3 was found to be at the plasma membrane (supplementary material Fig. S1A–C), whereas Kv1.5 was predominantly intracellular (supplementary material Fig. S1E–G). In addition, Kv1.3 currents were twofold higher than those of Kv1.5 under similar conditions (supplementary material Fig. S1D,H). This distribution is similar to that observed in other neuronal channels. Thus, Kv1.1 (supplementary material Fig. S2A–C) and Kv1.5 exhibited equivalent intracellular retention. In contrast, Kv1.4 (supplementary material Fig. S2D–F) and Kv1.3 exhibited analogous plasma membrane-associated patterns.

Several molecular determinants influence the localization of Kv1 channels in mammalian neurons. An ERR signature is present within the Kv1.1 pore, a FT motif (VxxSL) can be found at the C-terminus of Kv1.4. A P-loop sequence analysis (supplementary material Fig. S2G) indicates that neither Kv1.3 nor Kv1.5 contained the amino acids responsible for the intracellular retention of Kv1.1 (A352, E353, S369 and Y379) (Manganas et al., 2001b; Zhu et al., 2001). Furthermore, an analysis of C-termini demonstrated that the Kv1.4 FT signature ($V^{619}KESL^{623}$) was less functionally robust in Kv1.5

($L^{638}RRSL^{642}$) and absent in Kv1.3 (supplementary material Fig. S2H) (Li et al., 2000; Zhu et al., 2003; Steele et al., 2007).

To identify the motifs involved in Kv1.3 trafficking, Kv1.3/Kv1.5 chimeras were generated. Fig. 1 shows that a Kv1.3 with the Kv1.5 N-terminal (Fig. 1E–H) targeted to the membrane in a similar way to the Kv1.3 wild-type channels (Fig. 1A–D). However, when the C-terminus of Kv1.3 was replaced by that of Kv1.5 (Fig. 1I–L), the channel was retained intracellularly in a pattern similar to the Kv1.5 wild-type channel (Fig. 1M–P). These results indicated that the C-terminus of Kv1.3 is responsible for targeting Kv1.3 to the membrane. The reciprocal chimeras did not exhibit greater Kv1.5 surface expression, suggesting that the Kv1.3 element is not sufficient for normal Kv1.5 membrane surface expression and that potent ERR signatures must exist in Kv1.5.

To further study whether the Kv1.3 C-terminus was sufficient to promote membrane targeting, we generated a Kv1.3 lacking the complete C-terminus (93 residues). Unlike Kv1.3 (supplementary material Fig. S3A,B), Kv1.3(F433X) mistargeted the membrane surface and evoked no K^+ currents (supplementary material Fig. S3C,D). In addition, whereas Kv1.3 was highly expressed at the membrane and colocalized with the Golgi apparatus (supplementary material Fig. S3E–G), Kv1.3(F433X) remained at the ER (supplementary material Fig. S3H–J). Therefore, the Kv1.3 C-terminus contains signals that are essential for the proper delivery of the channels to the cell surface.

A di-acidic signature is sufficient to promote Kv1.3 localization at the cell membrane

To identify the Kv1.3 C-terminal signature responsible for targeting, we generated step-wise truncated channel proteins. We generated Kv1.3 channels lacking the final 34 (F492X), 39
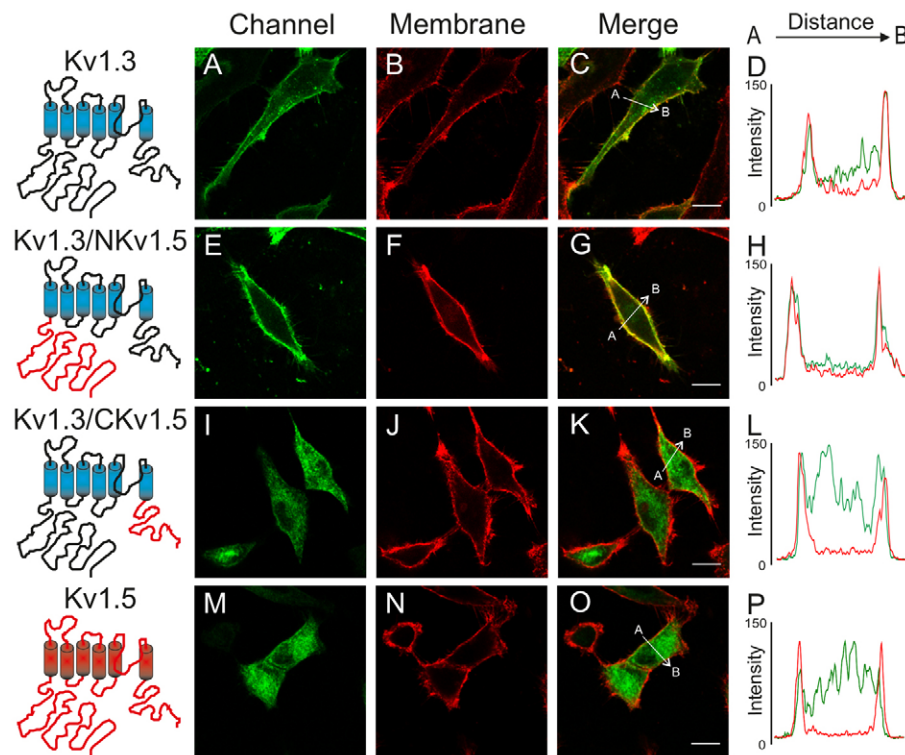

Fig. 1. The C-terminus of Kv1.5 impairs Kv1.3 membrane surface targeting. Confocal images demonstrate the distinct cellular distributions of the Kv1.3/Kv1.5 chimeras. Schematic diagrams of the channels are shown on the left. Kv1.3 is shown as blue transmembrane domains and black loops; Kv1.5 is shown as red transmembrane domains and red loops. (A–D) Kv1.3 is robustly expressed at the membrane surface. (A,E,I,M) Channel, (B,F,J,N) wheat germ agglutinin (WGA) staining of the plasma membrane, (C,G,K,O) merged image and (D,H,L,P) histogram showing the results of the pixel-by-pixel analysis of the section indicated by the arrow in the merged image. (E–H) Kv1.3/NKv1.5 colocalizes with WGA. (I–L) Kv1.3/CKv1.5 shows little colocalization with WGA. (M–P) Kv1.5 does not colocalize with WGA. Unlike A–H, little colocalization between the channels and WGA was observed in I–P. Although the Kv1.5 N-terminus did not mistarget the Kv1.3 channel to the surface, the C-terminal domain of Kv1.5 impaired the plasma membrane expression of Kv1.3. In all panels: green, channel; red, WGA; yellow, colocalization. Scale bars: 10 μm.

(M487X), 43 (E483X), 48 (E478X), 84 (E442X) and 93 (F433X, the entire C-terminus) residues (Fig. 2A). The progressive removal of residues from the Kv1.3 C-terminus yielded proteins that gradually decreased in size and that displayed altered glycosylation (Fig. 2B). Remarkably, the deletion of up to 39 residues at the far end of the C-terminus (wt, F492X and M487X) led to two major bands on western blots corresponding to mature glycosylated and immature non-glycosylated channels. The further removal of four or more amino acids (E483X, E478X, E442X and F433X) fully abolished channel glycosylation.

Fig. 2G,H shows that F492X and M487X were localized at the membrane. The distribution of M487X (Fig. 2I) was similar to that of the Kv1.3wt (see supplementary material Fig. S1A–D). In contrast, the deletion of four additional residues in the E483X channel severely impaired the surface expression (Fig. 2E,F). Kv1.3 mutants with further truncations (E478X and E442X) exhibited similar properties (Fig. 2C,D). Analysis of the Kv1.3 proteins and the membrane marker overlay revealed that less than 40% of the E483X channels were at the membrane. This membrane expression was similar to that observed for the Kv1.3 mutants with more severe truncations (Fig. 2J).

K^+ currents evoked by Kv1.3wt, F492X, E483X and F433X channels substantiated these observations (Fig. 2K,M). Although M487X currents were similar to those generated by Kv1.3wt, E483X currents were 85% lower than those evoked by the wt and M487F channels. Furthermore, E483X-evoked currents were similar to those obtained with F433X, which has no C-terminus (Fig. 2K,M). The I–V plots and similar half-activation voltages

(26.1±1.8, 25.1±3.1, 32.2±0.7, 26.91±1.2 mV for Kv1.3, F433X, E483X and M487X, respectively) demonstrated that the deletion of the 43 amino acids at the C-terminus impaired Kv1.3 surface expression (Fig. 2L).

YxxΦ motifs (Φ being hydrophobic residues) are responsible in many proteins for endocytosis and/or transport in the early secretory pathway (Lai and Jan, 2006; Schwegmann-Wessels et al., 2004). Fig. 3A is a pictorial representation of the YMVIEE motif, which may be a FT signal for Kv1.3. Interestingly, although both the M487X and E483X mutants contain the YMVI motif, M487X targeted to the cell surface, whereas E483X remained intracellular. This suggests that the absence of E483/484 in the E483X mutant is crucial for channel trafficking. To further define the Kv1.3 FT signature, we performed an alanine-scanning mutagenesis analysis of the YMVIEE cluster. No single- or double-alanine mutants, with the exception of those with an altered di-acidic E483E484 signature, exhibited impaired channel–membrane colocalization (Fig. 3H). However, the E483E484 to A483/484 substitution triggered intracellular retention (Fig. 3B–D,H). Intriguingly, a variety of mutations from VIEE to AAAA partially restored membrane expression (Fig. 3H). Because di-isoleucin motifs increase the intracellular retention, we generated a hydrophobic cluster by changing E483E484 to I483/484. The YMVIII mutation had severe consequences, and channels remained mostly intracellular, with the membrane colocalization 80% lower than that of Kv1.3wt (Fig. 3E–H). Although the YxxΦ was preserved in Kv1.3(YMVIAA) and Kv1.3(YMVIII) no apparent colocalization with EEA1 (early endosome-associated protein 1) was found (not shown).
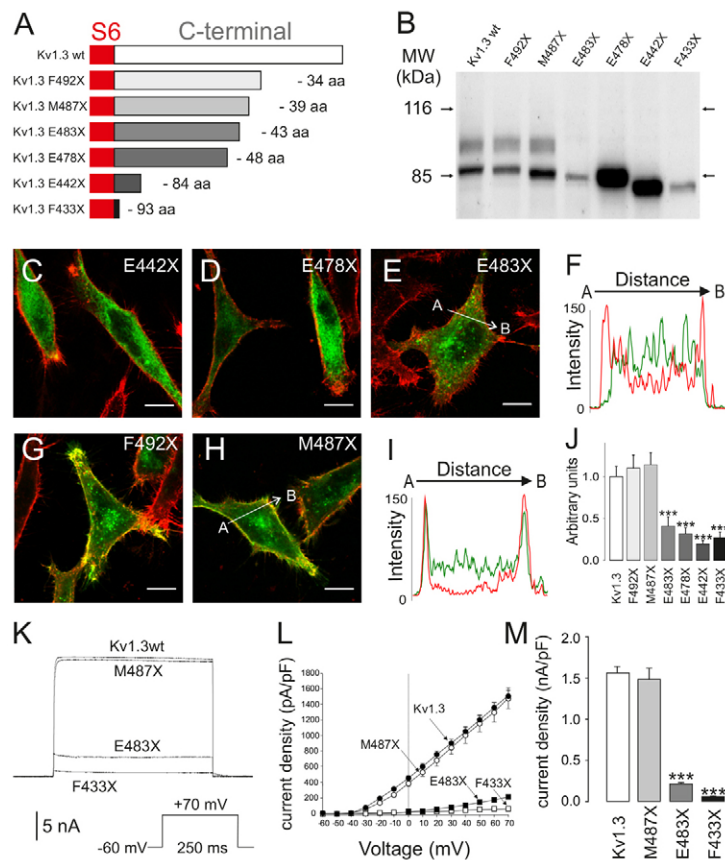
Fig. 2. Sequential Kv1.3 C-terminal domain truncation experiments reveal an important signaling element for membrane targeting and protein maturation. Kv1.3–YFP C-terminal truncations reveal an amino acid motif between M487 and E483 that participates in the anterograde transport, maturation and surface expression of Kv1.3. This motif has an important influence on cellular excitability. (A) A schematic diagram of the Kv1.3 C-terminal truncations. Red shows the position of the S6 transmembrane domain; the gradation from white to black represents the steady loss of residues. (B) Western blot analysis demonstrating that the progressive removal of amino acids reduces protein size and maturation. (C–E,G,H) Confocal images demonstrate that the sequential removal of residues split the channels into two categories. E442X (C), E478X (D) and E483X (C) are retained intracellularly in a pattern similar to F433X, which lacks the entire C-terminal domain, whereas, similar to Kv1.3wt, F492X (G) and M487X (H), which lack 34 and 39 aa, respectively, are targeted to the plasma membrane. (F,I) Histograms of the pixel-by-pixel analysis of the section indicated by the arrow in E (E483X) and H (M487X). Color code: green in all panels, channel; red, membrane; colocalization in yellow. Scale bars: 10 μm. (J) Membrane surface expressions of the truncated mutants. Pixel-by-pixel intensities from the confocal images were analyzed using ImageJ software. They were then compared with the relative intensity of the Kv1.3wt channel at the plasma membrane using a WGA overlay. Values are the means ± s.e.m. of at least 20 cells. (K–M) Sequential removal of residues from the Kv1.3 C-terminus severely impairs K^+ currents. (K) Representative traces. (L) Current–voltage dependence (pA/pF) of truncated mutants. (M) Current density (nA/pF). The cells were held at −60 mV, and currents were elicited by a single depolarizing pulse of 250 msecond duration to +70 mV (K and M) or similar depolarizing pulses in 10 mV steps (L). Values are the means ± s.e.m. of at least 10 cells. ***$P<0.001$ versus Kv1.3wt (Student's t-test).
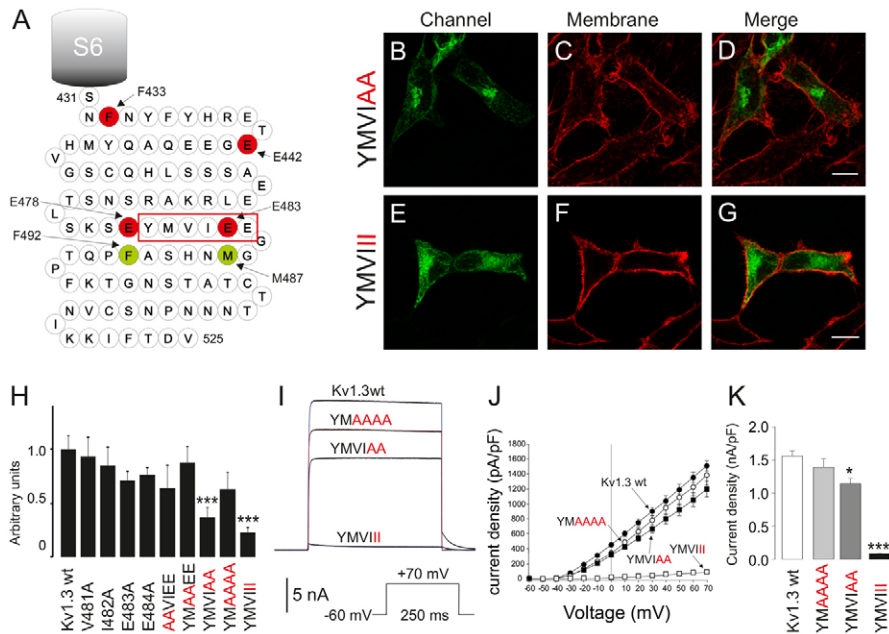
Fig. 3. Site-directed mutagenesis studies on the Y[479]MVIEE[484] motif. (A) Schematic diagram of the Kv1.3 C-terminal domain. The residues in green did not confer any harmful stops. In contrast, the amino acids in red conferred severe truncations. The S6 transmembrane domain is represented as a gray barrel. The YMVIEE cluster is indicated by the red box. (B–D) Confocal images demonstrating an impaired surface expression conferred by the substitution of E483/484 to Ala (YMVIAA). (E–G) Changes to I483/484 (YMVIII) almost abolished membrane targeting. Green, channel; red, WGA; merge, colocalization in yellow. Scale bars: 10 μm. (H) Membrane surface expression of mutated channels. Pixel-by-pixel intensities from the confocal images were analyzed using ImageJ software. Next, the results were compared with the relative intensity of the Kv1.3–YFP wt at the plasma membrane using a WGA overlay. Values are the means ± s.e.m. of at least 20 cells. Although ~50% of the YMVIAA mutant channels were expressed at the plasma membrane, YMVIII inhibited more than 70% of the surface expression. (I,J) Ala-scanning mutagenesis and Ile replacement of Glu at the YMVIEE motif impair K⁺ currents. (I) Representative traces. (J) Current–voltage dependence (pA/pF) of mutants. (K) Current density (nA/pF). The cells were held at −60 mV, and currents were elicited by a single depolarizing pulse of 250 msecond duration to +70 mV (I,K) or similar depolarizing pulses in 10 mV steps (J). Values are the means ± s.e.m. of at least 10 cells. *$P<0.05$, ***$P<0.001$ versus Kv1.3wt (Student's t-test). Mutations are indicated in red.

As expected, E483/484 mutations generated reduced K⁺ currents (Fig. 3I,K). The I–V plots and similar half-activation voltages (26.1±1.8, 24.2.±2.2, 28.8±2.3, 32.0±0.4 mV for Kv1.3, YMVAAAA, YMVIAA and YMVIII, respectively) demonstrated that the di-acidic E483/484 within the YMVIEE cluster at the C-terminus of Kv1.3 is a previously unrecognized FT signal that is responsible for channel trafficking to the cell surface.

Because Kv1.3 is important in sensory neurons (Rivera et al., 2005; Cavallin et al., 2010; Gazula et al., 2010) and leukocyte physiology (Vicente et al., 2003; Cahalan and Chandy, 2009) we analyzed the di-acidic E483/484 in neurons and lymphocytes. Rat embryo hippocampal neurons and Jurkat T-lymphocytes were transfected with Kv1.3wt and Kv1.3(I483/484). Whereas Kv1.3wt targeted to membranes and axons in neurons (Fig. 4A–C), Kv1.3 (I483/484) missed the axonal targeting and remained intracellular (Fig. 4D–F). Similarly, Kv1.3(I483/484) impaired the membrane surface expression in human T-lymphocytes (Fig. 4G,H). These observations further support that the E483/484 motif is essential for the delivery of the channels to the cell surface in neurons and lymphocytes.

Di-acidic signatures are present in neuronal Kv1 and Shaker channels

Is the YMVIEE motif conserved within the Kv1 and Shaker channels? We constructed a phylogenetic tree by comparing their C-terminal domains. Supplementary material Fig. S4 demonstrates that Kv1.1, Kv1.2 and Kv1.3 (neuronal channels) were in close proximity. Then, the distances enlarged (Kv1.5<Kv1.4=Kv1.6<Shaker=Kv1.7<Kv1.8). The proximity between Kv1.7 and Shaker channels is supported by Kv1.7 members from lizard (*Anolis carolinensis*) and a primitive coelacanth fish (*Latimeria chalumnae*) included in the Shaker cluster. Curiously, fish Kv1.7 members (*Tetraodon nigroviridis, Gasterosteus aculeatus* and *Takifugu rubripes*) are within the Kv1.8 cluster. Our data showed that most neuronal channels shared structural domains at the C-terminus (supplementary material Table S1). Therefore, we searched for YMVIEE motifs in Kv1 and Shaker subfamilies (Swiss-Prot, http://www.uniprot.org/). Similar YMVIEE signatures were present in neuronal Kv1.1 (YMEIEE), Kv1.2 (YMEIQE) and Kv1.4 (YLEMEE) (supplementary material Fig. S4B–E). Shakers exhibit a structurally homologous MDLDD consensus (supplementary material Fig. S4F). Notably, Kv1.5, a cardiac close relative of Kv1.1–Kv1.3, does not have the cluster, suggesting that this motif is restricted to neuronal Kv1 (supplementary material Table S1).

We analyzed Shaker and Kv1.1 channels to evaluate whether the di-acidic signature represents a general FT motif. Although Shaker wt (D532/533) partially targeted to the membrane (Fig. 5A–D), the mutant I532/533 showed a 60% reduction in membrane surface colocalization (Fig. 5E–H). Concomitantly, the Shaker mutant I532/533 exhibited K⁺ currents 50% lower
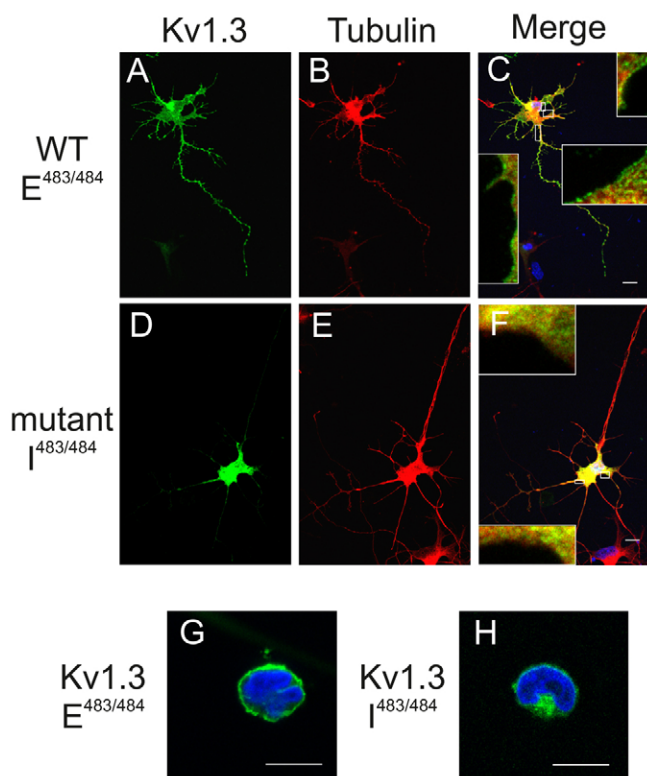
Fig. 4. The di-acidic E483/484 motif is important for axonal targeting and lymphocyte membrane surface expression. Hippocampal neurons from E17 rat embryos and Jurkat T-cells were cultured and transfected with Kv1.3wt (E483/484) and Kv1.3 mutant (E483/484I). (A–C) Kv1.3 wt targeted to axons. (A) Kv1.3 E483/484. (B) Neuron-specific class III-tubulin staining. (C) Merged image. (D–F) Kv1.3 (I483/484) mistargeted neuronal axons. (D) Kv1.3 mutant (I483/484). (E) Neuron-specific class III-tubulin. (F) merged image. Insets show enlarged views of the boxed regions. Scale bars: 10 μm. (G,H) The Kv1.3 mutant (I483/484) did not reach any membrane surface in human Jurkat T-lymphocytes. (G) Jurkat cell expressing Kv1.3 (E483/484). (H) Jurkat cell expressing Kv1.3 (I483/484). Scale bars: 5 μm. DAPI staining (in blue) was performed to highlight nuclei.

than Shaker wt (not shown). However, a P506 in the Kv1.4 pore, absent in Kv1.1 (A352), acts as a membrane surface expression motif (Manganas et al., 2001b). Unlike Kv1.4 (see supplementary material Fig. S2), Kv1.1 was intracellularly retained (Fig. 5I–L). However, the Kv1.1(A352P) mutation triggered a twofold increase in plasma membrane expression (Fig. 5M–P). Noteworthy, the additional mutation of the di-acidic motif in the A352P mutant (A352P/E458/459I) increased the channel retention by 50% (Fig. 5O–Q) and prevented the plasma membrane expression. In this vein, although the Kv1.2 channel also distributes intracellularly (Manganas and Trimmer, 2000), when we replaced the YMEIQE motif of Kv1.2 with YMVIEE, the Kv1.2(YMVIEE) mutant membrane targeting rose twofold (not shown). Collectively, these findings indicate that the newly identified di-acidic signature is a FT motif in mammalian neuronal Kv1.1, Kv1.2 and Shaker channels.

COPII-dependent mechanism of Kv1.3 anterograde transport

The secretory pathway of ion channels is uncertain. Whereas CFTR and hERG channels use COPII-coated vesicles to exit the

ER, Kv4.2 exits independently of COPII (Wang et al., 2004; Hasdemir et al., 2005; Delisle et al., 2009). We, therefore, questioned whether COPII was involved in Kv1.3 anterograde transport.

COPII vesicles include Sec23/Sec24 and Sec13/Sec31 heterodimers and Sar1 (Zanetti et al., 2012). Transfected Kv1.3wt cells were treated with brefeldin A for 24 hours, which resulted in Kv1.3 ER retention (Fig. 6A–F). Furthermore, inhibiting Sec13 recruitment by H89 increased Kv1.3 intracellular retention (Fig. 6G,H). The role of COPII was further supported by using the Sar1(H79G), which is a GTP-locked mutant that is a dominant negative and prevents the forward delivery of cargo proteins to the Golgi (Ward et al., 2001). Sar1(H79G) and Kv1.3 colocalized intracellularly (Fig. 6I–K) and were retained at the ER (Fig. 6L–O). Therefore, a COPII-dependent mechanism mediated the delivery of Kv1.3 to the cell surface.

We next analyzed association between COPII and the FT signature of the Kv1.3 C-terminus. Kv1.3wt showed little colocalization with Sec24D in cells co-transfected with both proteins (Fig. 7A–C). Similarly, the Kv1.3(E483X) mutant showed almost no colocalization with endogenous COPII vesicles (Fig. 7H–J). However, Sar1(H79G) triggered a notable Kv1.3-Sec24D-Sar1(H79G) intracellular colocalization (Fig. 7D–G). Furthermore, the presence of Sar1(H79G) increased the amount of Kv1.3 co-immunoprecipitated with Sec24D only when the Kv1.3 C-terminus was not disrupted (Fig. 7H). Sec24D did not significantly associate with E483X in the presence of Sar1(H79G), as revealed by the absence of Förster resonance energy transfer (FRET). However, Sar1(H79G) expression triggered FRET between Kv1.3wt and Sec24D. Therefore, alterations of the di-acidic E483/484 motif impairs molecular interactions between the channel and Sec24D (Fig. 7I).

To further understand the Kv1.3–Sec24 interaction at the molecular level, we used molecular modeling techniques. The transmembrane domain and the majority of the Kv1.3 N-terminus were homology modeled by using the Kv1.2 channel (PDB code 2R9R). The C-terminal domain shared significant similarity (~58%) with the nucleotide-binding domain of the reticulocyte-binding protein Py235 (3HGF) and the zinc-binding domain from neural zinc finger factor-1 (1PXE). Therefore, we used these proteins for building a molecular model of the Kv1.3 C-terminal region. The i-Tasser online server estimated a normalized Z-score of 0.92. Supplementary material Fig. S5A–C shows the side, top and bottom views of the full-length Kv1.3 model. In all three views, the YMVIEE cluster (depicted in red) in the C-terminus was accessible for protein–protein interactions. Fig. 8A–D shows a detailed view of the Kv1.3 C-terminal domain. The YMVIEE motif is a surface-exposed loop between two short alpha helices (Fig. 8A,B). Remarkably, the location of the E483/484 sequence suggested that this signature could easily establish saline bonds (Fig. 8B) with proteins such as Sec24. We next analyzed the docking of the Sec24a protein (PDB code 3EGD) to the Kv1.3 C-terminus in the model (Fig. 8C–E). Notably, Sec24a binds to vesicular stomatitis virus glycoprotein (VSVG). VSVG contains a characteristic YTDIEM cluster that is similar to the YMVIEE motif in Kv1.3. The main difference is that instead of the DxE signature in VSVG there is a VxE sequence in Kv1.3. Thus, the Asp is replaced by a hydrophobic residue. This change does not impact the interactions that are possible with either protein. As depicted in the model, I482 in Kv1.3 interacts with L498, L808 and V748 in Sec24a. In contrast, E483 in Kv1.3 establishes saline
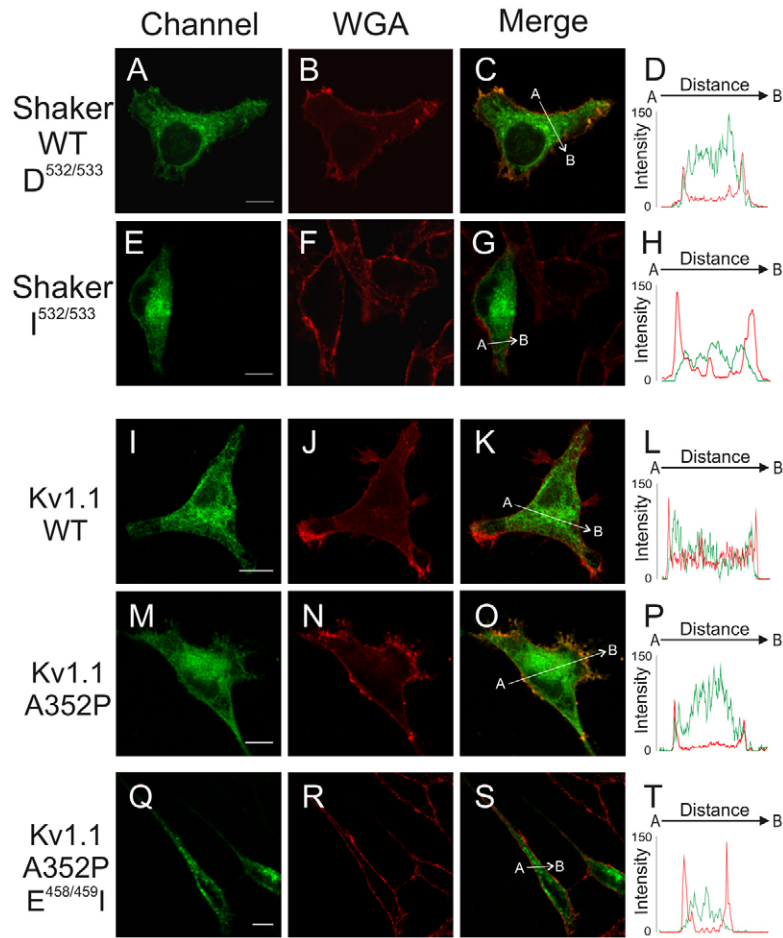
Fig. 5. **Analysis of di-acidic elements in Shaker and Kv1.1 channels.** (A–H) Shaker H4 wt D532/533 was mutated to I532/533 and membrane surface expression studied. (A–D) Shaker wt (D532/533) partially targeted to plasma membrane. (E–H) The I532/533 mutation impaired Shaker plasma membrane expression by 60% (*$P<0.05$ versus wt, Student's t-test). (I–T) The di-acidic E458/459 motif contributed to the Kv1.1 surface expression. (I–L) Kv1.1 wt was retained intracellularly. (M–P) Kv1.1(A352P) increased plasma membrane localization (**$P<0.01$ versus Kv1.1wt, Student's t-test). (Q–T) the triple mutant Kv1.1(A352P, E458/459I) restored the intracellular retention back to that of Kv1.1 wt (**$P<0.01$ versus A352P, Student's t-test). (D,H,L,P,T) Channel and WGA histograms. Pixel-by-pixel intensities from the confocal images were analyzed using ImageJ software. They were then compared with the relative intensity of the wt channels at the plasma membrane using the WGA overlay. Color code: green in all panels, channel; red, membrane WGA; yellow, colocalization in merged panels. Scale bars: 10 µm.

bonds with R752 and Y437 in Sec24a (Fig. 8D). The complex is further stabilized by the interactions of V497 and E484 in Kv1.3 with L773 and R750 in Sec24a, respectively (Fig. 8D). Note that the DxE signature that is responsible for Sec24a binding is replaced by the di-acidic E483/484 motif in the Kv1.3 C-terminus. Supporting this idea, I483/484 mutations in the di-acidic motif (YMVIII) fully disrupted the formation of saline bonds and prevented the binding of Sec24a to Kv1.3 (Fig. 8E). However, additional conformational changes should not be discounted.

Discussion

Kv1.3-mediated signaling is determined by the channel abundance at the cell surface. Thus, appropriate cellular trafficking and localization are crucial for the physiological roles of the Kv1.3 channels in sensory neurons and leukocytes. Alterations in these patterns are associated with autoimmune diseases and irregular axonal targeting (Rivera et al., 2005; Nicolaou et al., 2007; Steele et al., 2007; Tóth et al., 2009). Cumulative evidence suggests that the C-terminus of Kv channels plays crucial roles in their functionality as it contains domains implicated in protein trafficking to the cell surface, as well as ER retention (Curran et al., 1995; Neyroud et al., 1997; Biervert et al., 1998; Manganas et al., 2001a; Rea et al., 2002). Therefore, uncovering these signals is pivotal for understanding the molecular mechanisms underlying channel trafficking and surface expression in physiological and pathophysiological

conditions. Furthermore, this knowledge is fundamental for the development of therapeutic approaches to treat human diseases caused by dysfunctional channel expression.

The most salient contribution of this study is the identification of the Y[479]MVIEE[484] motif as a molecular determinant of the anterograde transport and membrane targeting of Kv1.3 channels. In particular, the di-acidic E483/484 signature within this motif is crucial for forward channel trafficking, as evidenced by the loss of channel transport to the cell surface upon its deletion or mutation. Analysis of the underlying mechanism involved in trafficking reveals that Kv1.3 traffics to the cell surface by a COPII-dependent pathway through interaction with Sec24. In fact, Kv1.3 traffics efficiently through the Golgi apparatus en route to the cell surface (Vicente et al., 2008). A molecular model of the Kv1.3–Sec24 complex suggests salt bridges between the E483/484 di-acidic signature at the Y[479]MVIEE[484] motif of the channel and a di-basic R750/752 signature in Sec24. Taken together, these findings unveil a novel trafficking signal in the Kv1.3 C-terminus that appears to underlie the high expression of this channel in the plasma membrane.

Notably, this mechanism appears conserved because this signature is also present in neuronal Kv1 and Shaker subfamilies. However, unlike Kv1.3, the presence of this di-acidic motif in neuronal Kv1 channels does not suffice to efficiently trigger their surface expression as these channels display a significant ER location. This lower trafficking efficiency in Kv1.1 and Shaker, as compared with Kv1.3, arises
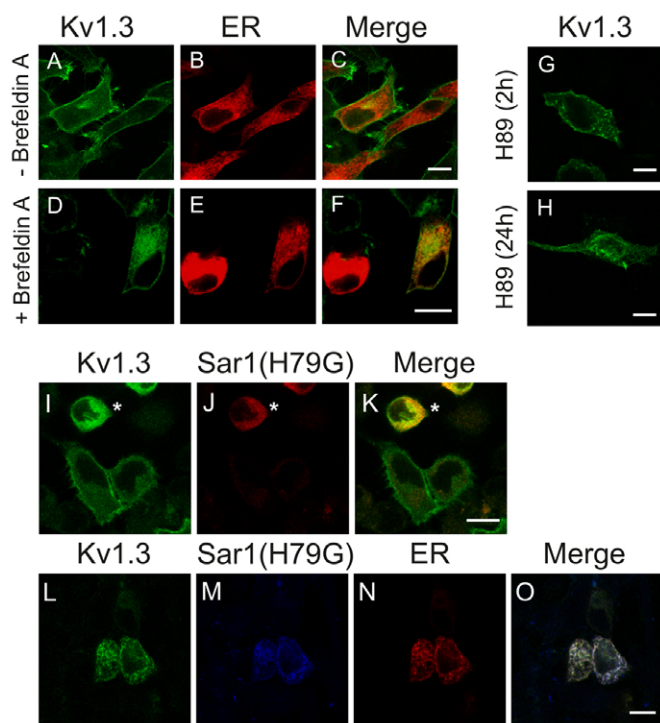
Fig. 6. Interfering with the COPII machinery impairs Kv1.3 trafficking and membrane surface targeting. (A–F) HEK-293 cells transiently transfected with Kv1.3-YFP and pDsRed-ER were treated in the absence (−) or the presence (+) of 10 µg/ml brefeldin A. (A–C) Kv1.3 did not colocalize with ER. (D–F) The presence of brefeldrin A triggered protein retention in the ER. Green, Kv1.3; red, pDsRed–ER; merge, yellow colocalization in merged panels. (G,H) The presence of 100 µg/ml H89 for 2 hours did not modify Kv1.3 membrane expression, but treatment for 24 hours resulted in the intracellular retention of the channel. (I–O) Expression of the constitutively active Sar1(H79G) dominant-negative GTPase also triggers the retention of Kv1.3 in the ER. (I–K) Kv1.3 and Sar1(H79G) colocalize. (I) Kv1.3 in green, (J) Sar1(H79G) in red, (K) colocalization in yellow. Note that the top cell marked with an asterisk co-expresses both proteins. The bottom cells, which do not express Sar1(H79G), target the Kv1.3 channels to the membrane. (L–O) The presence of Sar1(H79G) confines Kv1.3 at the ER. (L) Kv1.3 in green, (M) Sar1(H79G) in blue, (N) pDsRed–ER in red, (O) merged image, with white indicating triple colocalization. Scale bars: 10 µm.

most probably from a balance between this FT element and ERR motifs coexisting in their structures. Indeed, positive and negative FT elements have been characterized in several Kv1 channels. Whereas the A352 residue within the Kv1.1 pore inhibits trafficking (Manganas et al., 2001b; Zhu et al., 2001), an equivalent P505 in Kv1.4 favors surface expression (Li et al., 2000; Manganas et al., 2001b; Zhu et al., 2001). The A352P substitution in Kv1.1 causes enhanced currents and surface expression compared with wild-type Kv1.1 (Manganas et al., 2001b). However, these elements are not sufficient for the targeting of Kv1.4 to the cell membrane. In fact, the surface expression of Kv1.4(YLEMII) mutant did not apparently change (not shown). Therefore, the Kv1.4 requires the crucial contribution of the VxxSL signature in the channel C-terminus (Li et al., 2000; Zhu et al., 2003). This FT motif is absent in Kv1.3. Kv1.3 contains several dibasic ERR elements, including RxR ($R^{86}MR^{88}$, $R^{101}NR^{103}$ and $R^{118}IR^{120}$) in the N-terminus, KKxx ($K^{519}KIF^{522}$) in the C-terminus, and P^{374} in the P-loop.

However, mutation or deletion of these putative signals gave rise to inconclusive results and our data indicated that the Kv1.3 C-terminus must contain new and potent molecular FT determinants that act as signals for anterograde transport. This tenet was supported by the findings that Kv1.3(F433X) and the Kv1.3/Kv1.5 C-terminal chimera were not trafficked to the cell surface, suggesting that there are no FT sequences in the N-terminus or that inhibitory elements, such as the previously mentioned dibasic residues in this domain, act as dominant signals in the absence of the Kv1.3 C-terminus. Thus, the channel abundance at the cell surface is determined by the balance and strength of FT and ERR signals present in intracellular domains of the channels (Misonou and Trimmer, 2004).

A question that emerges is how this newly identified atypical di-acidic trafficking motif interacts with Sec24 to drive channel export from the ER to the plasma membrane. To address this question we modeled the complex formed by the Kv1.3 C-terminus and Sec24. In the absence of an atomic structure for the C-terminus of Kv1.3, we created a model that fulfilled all the structure–function available information and that was compatible with the reported density map at 23 Å-resolution of the Shaker channel (Sokolova et al., 2001; Sokolova et al., 2003). Thereafter, this model was docked into the atomic structure of the Sec24 protein, and energy minimized to have a picture of the complex. Although models have to be interpreted with caution, they represent very useful and testable tools for understanding molecular events. The proposed molecular model of the Kv1.3 channel suggests that its C-terminal domain can accommodate the four consecutive short alpha helices holding a water-exposed loop containing the YMVIEE motif, which is involved in Sec24 binding. Furthermore, the model highlights that the di-acidic motif forms salt bridges with two basic amino acids in the Sec24 protein and the hydrophobic residues contribute to stabilize the interaction of the complex. Notably, it has been reported that three consecutive hydrophobic residues ($V^{569}MI^{571}$) at the C-terminus of the GABA-1 transporter are responsible for exporting the protein from the endoplasmic reticulum–Golgi intermediate compartment (ERGC) (Farhan et al., 2008). Mutations in this motif are predicted to disrupt or destabilize the protein complex inhibiting COPII assembly and channel trafficking. Thus, the $Y^{479}MVI^{482}$ motif in Kv1.3 is also a hydrophobic domain that may play a similar role. In addition, the E483/484 di-acidic signature following this motif probably compensates for the absence of a canonical DxE and stabilizes the protein–protein interactions of Kv1.3 with its interacting partners, such as Sec24. In support of this tenet, clusters of acidic residues (e.g. ELETEEEE or EEEEDSE) act as post-Golgi surface-promoting signals in Kir channels without an obvious consensus sequence (Ma et al., 2002).

The identification of the molecular determinants responsible for normal channel function is essential for understanding their roles in health and disease. For example, in cystic fibrosis (CF) the CF transmembrane conductance regulator (CFTR) F508 mutant is misprocessed and intracellularly retained (Kartner et al., 1992). The forward trafficking of CFTR from the ER to the Golgi apparatus is dependent on COPII coat assembly in mammalian cells (Wang et al., 2004; Tsigelny et al., 2005). COPII proteins mediate the anterograde transport of cargo proteins to the cell membrane through the recognition of certain di-leucine and di-acidic motifs (Zanetti et al., 2012). For instance, the transport of the CFTR channel to the plasma membrane depends on a DxD
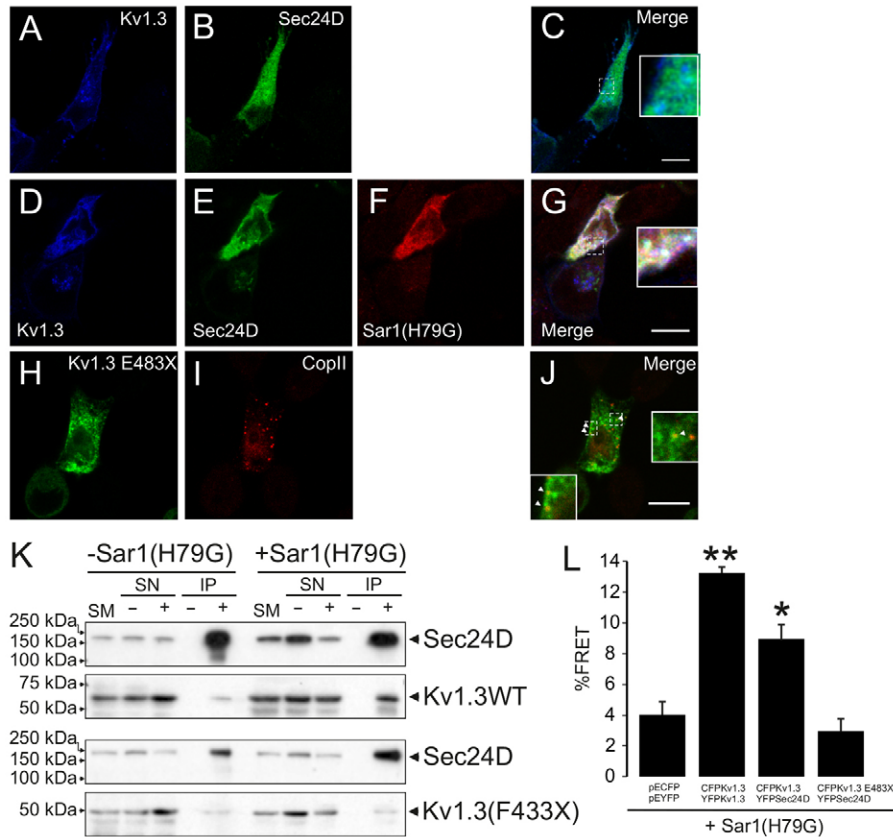
Fig. 7. Kv1.3 colocalizes with Sec24D in the presence of Sar1(H79G) and interacts with COPII as long as the di-acidic E483/484 motif is intact.
(A–C) Kv1.3–CFP and Sec24D–YFP showed limited colocalization. (D–G) The presence of Sar1(H79G) triggered Kv1.3 ER-retention and colocalization with Sec24D. (A,D) Kv1.3, (B,E) Sec24D, (F) Sar1(H79G), (C,G) merged images. White indicates triple colocalization. (H–J) Kv1.3-YFP(E483X), which lacks the di-acidic E483/484 motif, barely colocalizes with endogenous COPII. (H) Kv1.3(E483X), (I) COPII, (J) merged image. Insets, Enlarged views of COPII vesicles marked with the arrowheads. Scale bars: 10 µm. (K,L) Kv1.3 interacts with COPII via the C-terminal domain. (K) HEK cells were transiently transfected with Kv1.3-HA, Kv1.3(F433X)-HA and Sec24D-YFP in the presence (+) or the absence (−) of Sar1(H79G). Cell extracts were immunoprecipitated against YFP (Sec24D). Filters were blotted against HA (Kv1.3) and YFP (Sec24D). Sar1(H79G) expression notably increases the abundance of Kv1.3wt, but not Kv1.3(F433X), which co-immunoprecipitated with Sec24D–YFP. SM, starting material; SN, supernatant; IP, immunoprecipitate; +, presence of anti-GFP antibody; −, absence of anti-GFP antibody. (L) FRET experiments demonstrating the molecular interactions between Kv1.3–CFP and Sec24D–YFP in the presence of Sar1(H79G). Histogram shows the FRET efficiency of different combinations. Negative controls, cells expressing CFP and YFP; positive controls, cells expressing Kv1.3–CFP and Kv1.3–YFP. The E483X–CFP mutant shows no FRET with Sec24D–YFP indicating that no physical interactions take place in the absence of the E483/484 motif. $*P<0.05$; $**P<0.01$ versus CFP or YFP ($n=10$, Student's t-test).

signature in the C-terminus of the protein (Wang et al., 2004). This DxD signature and other neighboring residues accelerate ER export. These signals have also been identified in the vesicular stomatitis virus glycoprotein (VSVG) (Nishimura and Balch, 1997). The YTDIEM motif present in the VSVG is similar to that in the CFTR channel (YKDAD) (Sevier et al., 2000; Wang et al., 2004). Similarly, a congenital hyperinsulinism disease is caused by the E282K mutation of a DxE trafficking motif in the inward rectifying potassium channel Kir6.2 (Sivaprasadarao et al., 2007). This mutation disrupts a DxE motif and prevents the channel from assembling into COPII through complexing with Sec24. Lack of formation of this complex results in the retention of the protein in the ER and in a decrease in the number of Kir6.2 channels at the cell surface, which accounts for the disease phenotype (Sivaprasadarao et al., 2007; Taneja et al., 2009).

In summary, we reported the identification of a previously unrecognized FT protein motif (YMVIEE) in the C-terminus of Kv1.3, which is highly homologous in most neuronal Kv1 and Shaker subfamilies. This domain is essential for COPII-mediated

anterograde transport and the expression of the channel into the plasma membrane. Accordingly, alteration of the integrity of this novel molecular determinant of Kv1.3 trafficking gives rise to impaired channel expression, which may give rise to disease. The functioning of ion channels depends on both the activity control and the regulation of their abundance at the cell surface. Therefore, our data will help to understand pathologies associated to Kv1.3 such as autoimmune diseases, sensory neuron physiology, insulin resistance, obesity, hypertension and cancer. Thus, identifying the molecular determinants of Kv1.3 channel trafficking are of considerable interest and can aid to our understanding of channel function under physiological and pathological conditions. Furthermore, our findings point to Kv1.3 trafficking as a pharmacological target for drug development.

Materials and Methods
Expression plasmids and site-directed mutagenesis
Rat Kv1.3 in pRcCMV was provided by T.C. Holmes (New York University, NY). Rat Kv1.1 and Kv1.4 in pGEM7 and human Kv1.5 in pBK constructs were from M. M. Tamkun (Colorado State University, CO). Channels were subcloned into
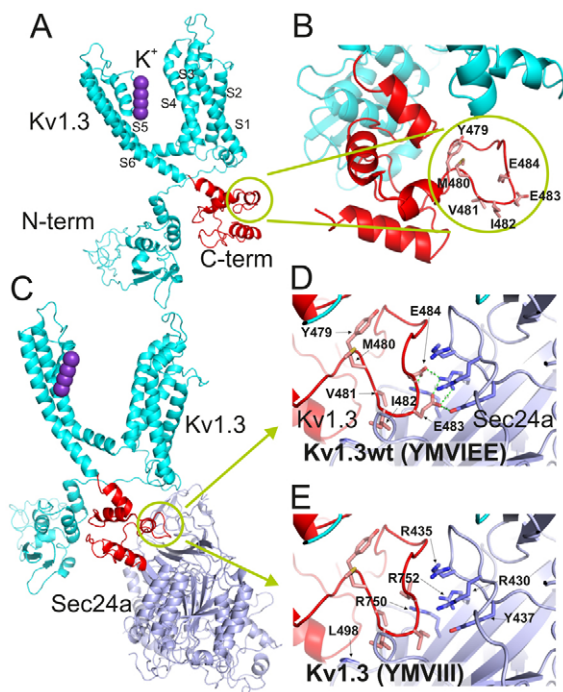
Fig. 8. Molecular dynamics simulation of the Kv1.3 C-terminal domain. (A–C) Molecular model of the Kv1.3 C-terminal domain. (A) A model of one Kv1.3 monomer is shown to highlight the surface-exposed loop structure. S1–S6 transmembrane domains (in cyan) and K$^+$ ions (in purple) are depicted for reference. The condensed C-terminal domain (in red), which contains four short alpha helices, is located on the side of the N-terminus (in cyan). (B) A detailed view of the surface-exposed YMVIEE loop structure. (C) Molecular recognition of the Kv1.3 C-terminus and the Sec2a subunits of COPII. The YMVIEE loop structure is circled in green. (D,E) Two views of the Kv1.3 C-terminus bound to Sec24d. Docking simulation identified potential sites of interaction between Sec24a and the YMVIEE motif of Kv1.3. Saline and hydrogen bonds are formed between E483/484 in Kv1.3 and R752, R750 and Y437 in Sec24a. These bonds are depicted by the green dashed lines. (D) YMVIEE in the Kv1.3 wt channels. (E) YMVIII in the Kv1.3 mutant channel illustrates the absence of interactions.

pEYFP-C1 and pECFP-C1 (Clontech). Constructs were verified by sequencing. The rKv1.3, externally tagged with HA between S3 and S4, was from D. B. Arnold (University of Southern California, CA). The pEYFP-Sec24D and the HA-Sar1(H79G) were from T. H. Ward (The London School of Hygiene and Tropical Medicine, UK) and R. Pepperkok (EMBL, Heidelberg, Germany), respectively. All Kv1.3 mutants and Kv1.3/Kv1.5 chimeras were generated in the pEYFP-Kv1.3, Kv1.3HA and pEYFP-Kv1.5 channels. Golgi (pECFP–Golgi) and ER (pDsRed–ER) markers were from Clontech. The Shaker H4 channel in pQBI25-fC3 was used for this study. All Shaker constructs, including the one referred to as 'wild type', contained a deletion of residues 6–46 to remove fast inactivation (Hoshi et al., 1990).

Kv1.3–Kv1.5 chimeras were generated by inserting *Bgl*II and *Eco*RI sites in the N- and C-terminal domains of the channels, respectively. Using restriction sites, truncations and single and multiple Kv1.1, Kv1.3 and Shaker mutants were generated using the QuikChange and QuikChange multi-site-directed mutagenesis kits (Stratagene). All mutations were verified using automated DNA sequencing.

Cell culture and transient transfections

HEK-293 cells were grown in DMEM containing 10% FBS and 100 U/ml penicillin and streptomycin. For the confocal analyses, cells cultured in the same medium were plated on poly-lysine-coated coverslips. Transient transfection was performed using MetafecteneTM Pro (Biontex) at nearly 80% confluency. Jurkat T-lymphocytes were cultured in RPMI culture medium, containing 10% FBS and supplemented with 10 U/ml penicillin and streptomycin and 2 mM L-glutamine. Transient transfection was performed by electroporation (Bio-Rad). Twenty-four hours after transfection, cells were washed in phosphate-buffered saline (PBS;

without K$^+$), fixed with 4% paraformaldehyde in PBS for 10 minutes and mounted with Aqua Poly/Mount (Polysciences). In some experiments, Kv1.3-transfected cells were treated with 10 µg/ml brefeldin A (an inhibitor of a GTP–GDP exchange enzyme that impairs the release of ADP-ribosylating factor and COPII from the Golgi apparatus) and 100 µg/ml H89 (a selective protein kinase A inhibitor that prevents the recruitment of COPII to the ER export sites through Sec13-mediated mechanisms).

Dissociated and explant cultures of neurons

The hippocampus of E17 rat embryos was dissected out to obtain primary neuronal cultures. All animal experiments were performed according to approved guidelines. After trypsin–EDTA (0.05% trypsin, 0.53 mM EDTA, 12 minutes; Invitrogen) and DNase1 (100 U/ml, 10 minutes; Roche Diagnostics) treatments, tissue was dissociated by gentle stirring. 50,000 cells were cultured for 3 days onto poly-L-lysine-coated dishes in neurobasal medium containing L-glutamine, penicillin and streptomycin and B27 supplement (Invitrogen). Thirty-six hours after plating, neurons were transfected with pEYFP-Kv1.3 or pEYFP-Kv1.3YMVIII using Lipofectamine 2000 (Invitrogen). Hippocampal neurons were immunostained with an antibody against neuron-specific class III β-tubulin (clone TUJ-1; 1:4000; Sigma), followed by Alexa Fluor 568 secondary antibody (1:500; Molecular Probes) were processed as above.

Protein extraction, co-immunoprecipitation and western blot analysis

Cells, washed in cold PBS, were lysed on ice with NHG solution (1% Triton X-100, 10% glycerol, 50 mmol/l HEPES pH 7.2, 150 mmol/l NaCl) supplemented with 1 µg/ml aprotinin, 1 µg/ml leupeptin, 1 µg/ml pepstatin and 1 mM phenylmethylsulfonyl fluoride to inhibit proteases. Homogenates were centrifuged at 16,000 *g* for 15 minutes, and the protein content was measured using the Bio-Rad Protein Assay.

The samples were precleared with 30 µl of protein-G–Sepharose beads for 2 hours at 4℃ with gentle mixing as part of the co-immunoprecipitation procedures. The beads were then removed by centrifugation at 1000 *g* for 30 seconds at 4℃. Samples were incubated overnight with the desired antibody (4 ng/µg protein) at 4℃ with gentle agitation. Thirty microliters of protein-G–Sepharose were then added to each sample and they were incubated for 4 hours at 4℃. The beads were removed by centrifugation at 1000 *g* for 30 seconds at 4℃, washed four times in NHG, and resuspended in 80 µl SDS sample buffer.

Protein samples (50 µg) and immunoprecipitates were boiled in Laemmli SDS loading buffer and separated by 10% SDS-PAGE. Next, the samples were transferred to nitrocellulose membranes (Immobilon-P, Millipore) and blocked in 5% dry milk supplemented with 0.05% Tween 20 in PBS before the immunoreaction. The filters were then immunoblotted with antibodies against HA (1/200, Sigma) and GFP (1/1000, Roche).

Confocal microscopy and FRET

Staining with wheat germ agglutinin (WGA–Texas Red®; Invitrogen) to label the plasma membrane was performed under non-permeabilized conditions. Cells were washed with PBS and stained for 30 minutes at 4℃. Next, cells were washed and fixed with 4% paraformaldehyde in PBS for 10 minutes. To detect the COPII protein, cells were further permeabilized using 0.1% Triton X-100 for 10 minutes. After a 60 minute incubation with a blocking solution (10% goat serum, 5% non-fat dry milk, PBS), the cells were treated with an anti-COPII polyclonal antibody (1:250; ABR) in 10% goat serum, 0.05% Triton X-100 and again incubated for 1 hour. Then, the cells were further incubated for 45 minutes with an Alexa-Fluor-555 antibody (1:500; Molecular probes). All experiments were performed at room temperature.

The acceptor photobleaching technique was applied to measure the Förster resonance energy transfer (FRET). Fluorescent proteins from fixed cells were excited with the 458 nm or the 514 nm lines using low excitation intensities. Next, 475–495 nm bandpass and >530 nm longpass emission filters were applied. The YFP protein in half of each cell was bleached using maximum laser power. We obtained ~80% of acceptor intensity bleaching. After photobleaching, images of the donors and acceptors were taken. The FRET efficiency was calculated using the equation $[(F_{CFPafter}-F_{CFPbefore})/F_{CFPbefore}]\times100$, where $F_{CFPafter}$ was the fluorescence of the donor after bleaching and $F_{CFPbefore}$ was the fluorescence before bleaching. The loss of fluorescence as a result of the scans was corrected by measuring the CFP intensity in the unbleached part of the cell. FRET values were expressed as the mean and standard error of more than 15 cells for each group. Cells were examined with a 63× oil immersion objective on a Leica TCS SL laser scanning confocal microscope. All offline image analyses were performed using a Leica confocal microscope, ImageJ software and Sigmaplot.

Electrophysiology

Whole-cell currents were recorded using the patch–clamp technique in the whole-cell configuration with a HEKA EPC10 amplifier (HEKA Elektronik). PatchMaster software (HEKA) was used for data acquisition. A stimulation frequency of 50 kHz and a filter at 10 kHz was used. The capacitance and series resistance compensation were optimized. In most experiments, we obtained an

80% compensation of the effective access resistance. Micropipettes were made from borosilicate glass capillaries (Harvard Apparatus) using a P-97 puller (Sutter Instrument) and fire polished. Pipettes had a resistance of 2–4 MΩ when filled with a solution containing (in mM): 120 KCl, 1 CaCl$_2$, 2 MgCl$_2$, 10 HEPES, 10 EGTA, 20 D-glucose (pH 7.3 and 280 mOsm/l). The extracellular solution contained (in mM): 120 NaCl, 5.4 KCl, 2 CaCl$_2$, 1 MgCl$_2$, 10 HEPES and 25 D-glucose (pH 7.4 and 310 mOsm/l). Cells were clamped at a holding potential of −60 mV. To evoke voltage-gated currents, all cells were stimulated with 250-msecond square pulses ranging from −60 to +70 mV in 10 mV steps. The peak amplitude (pA) was normalized using the capacitance values (pF). Data analysis was performed using FitMaster (HEKA) and Sigma Plot 10.0 software (Systat Software). All recordings were performed at room temperature.

Kv1.3 channel modeling

The protein was modeled using high-resolution templates of remote or close homologs available from the Protein Data Bank (http://www.rcsb.org/pdb). The transmembrane domain and the N-terminus (except the first 49 amino acids) were modeled with the Kv1.2 potassium channel (PDB code 2R9R). The C-terminus and the remaining 49 amino acids from the N-terminus were modeled with 3HGF (nucleotide binding domain of the reticulocyte binding protein Py235) and 1PXE (zinc-binding domain from neural zinc finger factor-1) codes, respectively. This procedure has been outlined on the i-Tasser online server (http://zhanglab.ccmb. med.umich.edu/I-TASSER/). We then performed multiple sequence alignment using CLUSTALW (Thompson et al., 1994) from the European Bioinformatics Institute site (http://www.ebi.ac.uk). The homology modeling was performed using the Swiss-Model Protein Modeling Server (Schwede et al., 2003) on the ExPASy Molecular Biology website (http://kr.expasy.org/) under the *Project Mode*. Structure visualization and modifications were made using Yasara v11.6.16 (Krieger et al., 2002) and DeepView v4 (Guex and Peitsch, 1997). The orientation and optimization of the side chains were carried out in two steps. First, the residues showing van der Waals clashes were selected and fitted with the 'Quick and Dirty' algorithm (DeepView). Second, the models were energy minimized. This process involved an initial short steepest descent minimization to remove bumps. Next, we performed a simulated annealing minimization. In this procedure, the simulation cell was slowly cooled towards 0K by downscaling the atom velocities. The entire system was subject to an equilibration process before the molecular dynamics simulation. The equilibration consisted of an initial minimization of the fixed backbone atoms. Next, the restrained carbon alpha atoms were minimized and a short molecular dynamics (10 pseconds) minimization was performed. The goal of the latter step was to reduce the initial incorrect contacts and to fill the empty cavities. Finally, under periodic boundary conditions in the three coordinate directions, the full system was simulated at 310˚K for 0.5 nseconds. All dynamic simulations were performed using Yasara (Krieger et al., 2002) with the force field AMBER03 (Duan et al., 2003). The cut-off used for long-range interactions was set at 10 Å.

The resulting model was used to test for docking with the Sec24a structure (Mancias and Goldberg, 2008). This structure was extracted from the mammalian COPII-coat protein complex Sec23a/Sec24a/Sec22 bound to the transport signal sequence of the vesicular stomatitis virus glycoprotein (PDB code 3EGD) (Mancias and Goldberg, 2008). A local docking procedure was accomplished using AutoDock 4 (Morris et al., 2008). In this procedure, a total of 100 flexible docking runs were set and clustered around the YMVIEE motif in the C-terminus of the Kv1.3 channel. The binding energy of the docked complexes was obtained by calculating the energy between the channel and the transport protein at infinite distance and then subtracting the energy of the whole complex. The energy in each cluster was stored, analyzed, and applied to select the most likely orientation of the interacting proteins. The energy of the model and the docking complexes were tested using FoldX (Guerois et al., 2002; Schymkowitz et al., 2005) on the CRG site: http://foldx.crg.es. The force field of FoldX allowed us to evaluate the properties of the structure. Such parameters as the atomic contact map, the accessibility of the atoms and residues, the backbone dihedral angles, the hydrogen bonds and the electrostatic networks of the protein were assessed. In addition, the model was evaluated using PROCHECK to show the residues in the allowed regions of the Ramachandran plots (Laskowski et al., 1996). The final molecular graphic representations were created using PyMOL v1.4.1 (http://www. pymol.org/).

Author contributions

A.F. conceived and supervised the study and wrote the manuscript. R.M.M., M.P.V., S.R.R., A.V.G., P.G., A.S.A., M.I.B. and N.C.

conducted experiments. A.F.M. and G.F.B. performed the phylogenic analysis and the channel modeling. All authors contributed to data analysis, interpretation and commented on the manuscript.

Supplementary material available online at
http://jcs.biologists.org/lookup/suppl/doi:10.1242/jcs.134825/-/DC1

References

Biervert, C., Schroeder, B. C., Kubisch, C., Berkovic, S. F., Propping, P., Jentsch, T. J. and Steinlein, O. K. (1998). A potassium channel mutation in neonatal human epilepsy. *Science* **279**, 403-406.

Cahalan, M. D. and Chandy, K. G. (2009). The functional network of ion channels in T lymphocytes. *Immunol. Rev.* **231**, 59-87.

Cavallin, M. A., Powell, K., Biju, K. C. and Fadool, D. A. (2010). State-dependent sculpting of olfactory sensory neurons is attributed to sensory enrichment, odor deprivation, and aging. *Neurosci. Lett.* **483**, 90-95.

Conforti, L. (2012). The ion channel network in T lymphocytes, a target for immunotherapy. *Clin. Immunol.* **142**, 105-106.

Curran, M. E., Splawski, I., Timothy, K. W., Vincent, G. M., Green, E. D. and Keating, M. T. (1995). A molecular basis for cardiac arrhythmia: HERG mutations cause long QT syndrome. *Cell* **80**, 795-803.

Delisle, B. P., Underkofler, H. A., Moungey, B. M., Slind, J. K., Kilby, J. A., Best, J. M., Foell, J. D., Balijepalli, R. C., Kamp, T. J. and January, C. T. (2009). Small GTPase determinants for the Golgi processing and plasmalemmal expression of human ether-a-go-go related (hERG) K+ channels. *J. Biol. Chem.* **284**, 2844-2853.

Duan, Y., Wu, C., Chowdhury, S., Lee, M. C., Xiong, G., Zhang, W., Yang, R., Cieplak, P., Luo, R., Lee, T. et al. (2003). A point-charge force field for molecular mechanics simulations of proteins based on condensed-phase quantum mechanical calculations. *J. Comput. Chem.* **24**, 1999-2012.

Farhan, H., Reiterer, V., Kriz, A., Hauri, H. P., Pavelka, M., Sitte, H. H. and Freissmuth, M. (2008). Signal-dependent export of GABA transporter 1 from the ER-Golgi intermediate compartment is specified by a C-terminal motif. *J. Cell Sci.* **121**, 753-761.

Gazula, V. R., Strumbos, J. G., Mei, X., Chen, H., Rahner, C. and Kaczmarek, L. K. (2010). Localization of Kv1.3 channels in presynaptic terminals of brainstem auditory neurons. *J. Comp. Neurol.* **518**, 3205-3220.

Guerois, R., Nielsen, J. E. and Serrano, L. (2002). Predicting changes in the stability of proteins and protein complexes: a study of more than 1000 mutations. *J. Mol. Biol.* **320**, 369-387.

Guex, N. and Peitsch, M. C. (1997). SWISS-MODEL and the Swiss-PdbViewer: an environment for comparative protein modeling. *Electrophoresis* **18**, 2714-2723.

Hasdemir, B., Fitzgerald, D. J., Prior, I. A., Tepikin, A. V. and Burgoyne, R. D. (2005). Traffic of Kv4 K+ channels mediated by KChIP1 is via a novel post-ER vesicular pathway. *J. Cell Biol.* **171**, 459-469.

Hille, B. (2001). *Ion Channels of Excitable Membranes*. Sunderland, MA: Sinauer.

Hoshi, T., Zagotta, W. N. and Aldrich, R. W. (1990). Biophysical and molecular mechanisms of Shaker potassium channel inactivation. *Science* **250**, 533-538.

Kartner, N., Augustinas, O., Jensen, T. J., Naismith, A. L. and Riordan, J. R. (1992). Mislocalization of delta F508 CFTR in cystic fibrosis sweat gland. *Nat. Genet.* **1**, 321-327.

Koeberle, P. D. and Schlichter, L. C. (2010). Targeting K(V) channels rescues retinal ganglion cells in vivo directly and by reducing inflammation. *Channels (Austin)* **4**, 337-346.

Krieger, E., Koraimann, G. and Vriend, G. (2002). Increasing the precision of comparative models with YASARA NOVA—a self-parameterizing force field. *Proteins* **47**, 393-402.

Lai, H. C. and Jan, L. Y. (2006). The distribution and targeting of neuronal voltage-gated ion channels. *Nat. Rev. Neurosci.* **7**, 548-562.

Laskowski, R. A., Rullmann, J. A., MacArthur, M. W., Kaptein, R. and Thornton, J. M. (1996). AQUA and PROCHECK-NMR: programs for checking the quality of protein structures solved by NMR. *J. Biomol. NMR* **8**, 477-486.

Li, D., Takimoto, K. and Levitan, E. S. (2000). Surface expression of Kv1 channels is governed by a C-terminal motif. *J. Biol. Chem.* **275**, 11597-11602.

Ma, D., Zerangue, N., Raab-Graham, K., Fried, S. R., Jan, Y. N. and Jan, L. Y. (2002). Diverse trafficking patterns due to multiple traffic motifs in G protein-activated inwardly rectifying potassium channels from brain and heart. *Neuron* **33**, 715-729.

Mancias, J. D. and Goldberg, J. (2008). Structural basis of cargo membrane protein discrimination by the human COPII coat machinery. *EMBO J.* **27**, 2918-2928.

Manganas, L. N. and Trimmer, J. S. (2000). Subunit composition determines Kv1 potassium channel surface expression. *J. Biol. Chem.* **275**, 29685-29693.

Manganas, L. N., Akhtar, S., Antonucci, D. E., Campomanes, C. R., Dolly, J. O. and Trimmer, J. S. (2001a). Episodic ataxia type-1 mutations in the Kv1.1 potassium channel display distinct folding and intracellular trafficking properties. *J. Biol. Chem.* **276**, 49427-49434.

Manganas, L. N., Wang, Q., Scannevin, R. H., Antonucci, D. E., Rhodes, K. J. and Trimmer, J. S. (2001b). Identification of a trafficking determinant localized to the Kv1 potassium channel pore. *Proc. Natl. Acad. Sci. USA* **98**, 14055-14059.

Marks, D. R., Tucker, K., Cavallin, M. A., Mast, T. G. and Fadool, D. A. (2009). Awake intranasal insulin delivery modifies protein complexes and alters memory, anxiety, and olfactory behaviors. *J. Neurosci.* **29**, 6734-6751.

Misonou, H. and Trimmer, J. S. (2004). Determinants of voltage-gated potassium channel surface expression and localization in Mammalian neurons. *Crit. Rev. Biochem. Mol. Biol.* **39**, 125-145.

Morris, G. M., Huey, R. and Olson, A. J. (2008). Using AutoDock for ligand-receptor docking. *Curr. Protoc. Bioinformatics* **24**, 8.14.1–8.14.40.

Neyroud, N., Tesson, F., Denjoy, I., Leibovici, M., Donger, C., Barhanin, J., Fauré, S., Gary, F., Coumel, P., Petit, C. et al. (1997). A novel mutation in the potassium channel gene KVLQT1 causes the Jervell and Lange-Nielsen cardioauditory syndrome. *Nat. Genet.* **15**, 186-189.

Nicolaou, S. A., Szigligeti, P., Neumeier, L., Lee, S. M., Duncan, H. J., Kant, S. K., Mongey, A. B., Filipovich, A. H. and Conforti, L. (2007). Altered dynamics of Kv1.3 channel compartmentalization in the immunological synapse in systemic lupus erythematosus. *J. Immunol.* **179**, 346-356.

Nishimura, N. and Balch, W. E. (1997). A di-acidic signal required for selective export from the endoplasmic reticulum. *Science* **277**, 556-558.

Panyi, G., Vámosi, G., Bacsó, Z., Bagdány, M., Bodnár, A., Varga, Z., Gáspár, R., Mátyus, L. and Damjanovich, S. (2004). Kv1.3 potassium channels are localized in the immunological synapse formed between cytotoxic and target cells. *Proc. Natl. Acad. Sci. USA* **101**, 1285-1290.

Rea, R., Spauschus, A., Eunson, L. H., Hanna, M. G. and Kullmann, D. M. (2002). Variable K(+) channel subunit dysfunction in inherited mutations of KCNA1. *J. Physiol.* **538**, 5-23.

Rivera, J. F., Chu, P. J. and Arnold, D. B. (2005). The T1 domain of Kv1.3 mediates intracellular targeting to axons. *Eur. J. Neurosci.* **22**, 1853-1862.

Schwede, T., Kopp, J., Guex, N. and Peitsch, M. C. (2003). SWISS-MODEL: An automated protein homology-modeling server. *Nucleic Acids Res.* **31**, 3381-3385.

Schwegmann-Wessels, C., Al-Falah, M., Escors, D., Wang, Z., Zimmer, G., Deng, H., Enjuanes, L., Naim, H. Y. and Herrler, G. (2004). A novel sorting signal for intracellular localization is present in the S protein of a porcine coronavirus but absent from severe acute respiratory syndrome-associated coronavirus. *J. Biol. Chem.* **279**, 43661-43666.

Schymkowitz, J., Borg, J., Stricher, F., Nys, R., Rousseau, F. and Serrano, L. (2005). The FoldX web server: an online force field. *Nucleic Acids Res.* **33**, W382-W388.

Sevier, C. S., Weisz, O. A., Davis, M. and Machamer, C. E. (2000). Efficient export of the vesicular stomatitis virus G protein from the endoplasmic reticulum requires a signal in the cytoplasmic tail that includes both tyrosine-based and di-acidic motifs. *Mol. Biol. Cell* **11**, 13-22.

Sivaprasadarao, A., Taneja, T. K., Mankouri, J. and Smith, A. J. (2007). Trafficking of ATP-sensitive potassium channels in health and disease. *Biochem. Soc. Trans.* **35**, 1055-1059.

Sokolova, O., Kolmakova-Partensky, L. and Grigorieff, N. (2001). Three-dimensional structure of a voltage-gated potassium channel at 2.5 nm resolution. *Structure* **9**, 215-220.

Sokolova, O., Accardi, A., Gutierrez, D., Lau, A., Rigney, M. and Grigorieff, N. (2003). Conformational changes in the C terminus of Shaker K+ channel bound to the rat Kvbeta2-subunit. *Proc. Natl. Acad. Sci. USA* **100**, 12607-12612.

Steele, D. F., Zadeh, A. D., Loewen, M. E. and Fedida, D. (2007). Localization and trafficking of cardiac voltage-gated potassium channels. *Biochem. Soc. Trans.* **35**, 1069-1073.

Taneja, T. K., Mankouri, J., Karnik, R., Kannan, S., Smith, A. J., Munsey, T., Christesen, H. B., Beech, D. J. and Sivaprasadarao, A. (2009). Sar1-GTPase-dependent ER exit of KATP channels revealed by a mutation causing congenital hyperinsulinism. *Hum. Mol. Genet.* **18**, 2400-2413.

Thompson, J. D., Higgins, D. G. and Gibson, T. J. (1994). CLUSTAL W: improving the sensitivity of progressive multiple sequence alignment through sequence weighting, position-specific gap penalties and weight matrix choice. *Nucleic Acids Res.* **22**, 4673-4680.

Tóth, A., Szilágyi, O., Krasznai, Z., Panyi, G. and Hajdú, P. (2009). Functional consequences of Kv1.3 ion channel rearrangement into the immunological synapse. *Immunol. Lett.* **125**, 15-21.

Tsigelny, I., Hotchko, M., Yuan, J. X. and Keller, S. H. (2005). Identification of molecular determinants that modulate trafficking of DeltaF508 CFTR, the mutant ABC transporter associated with cystic fibrosis. *Cell Biochem. Biophys.* **42**, 41-53.

Vicente, R., Escalada, A., Coma, M., Fuster, G., Sánchez-Tilló, E., López-Iglesias, C., Soler, C., Solsona, C., Celada, A. and Felipe, A. (2003). Differential voltage-dependent K+ channel responses during proliferation and activation in macrophages. *J. Biol. Chem.* **278**, 46307-46320.

Vicente, R., Villalonga, N., Calvo, M., Escalada, A., Solsona, C., Soler, C., Tamkun, M. M. and Felipe, A. (2008). Kv1.5 association modifies Kv1.3 traffic and membrane localization. *J. Biol. Chem.* **283**, 8756-8764.

Villalonga, N., David, M., Bielańska, J., González, T., Parra, D., Soler, C., Comes, N., Valenzuela, C. and Felipe, A. (2010). Immunomodulatory effects of diclofenac in leukocytes through the targeting of Kv1.3 voltage-dependent potassium channels. *Biochem. Pharmacol.* **80**, 858-866.

Wang, X., Matteson, J., An, Y., Moyer, B., Yoo, J. S., Bannykh, S., Wilson, I. A., Riordan, J. R. and Balch, W. E. (2004). COPII-dependent export of cystic fibrosis transmembrane conductance regulator from the ER uses a di-acidic exit code. *J. Cell Biol.* **167**, 65-74.

Ward, T. H., Polishchuk, R. S., Caplan, S., Hirschberg, K. and Lippincott-Schwartz, J. (2001). Maintenance of Golgi structure and function depends on the integrity of ER export. *J. Cell Biol.* **155**, 557-570.

Zanetti, G., Pahuja, K. B., Studer, S., Shim, S. and Schekman, R. (2012). COPII and the regulation of protein sorting in mammals. *Nat. Cell Biol.* **14**, 20-28.

Zhu, J., Watanabe, I., Gomez, B. and Thornhill, W. B. (2001). Determinants involved in Kv1 potassium channel folding in the endoplasmic reticulum, glycosylation in the Golgi, and cell surface expression. *J. Biol. Chem.* **276**, 39419-39427.

Zhu, J., Watanabe, I., Gomez, B. and Thornhill, W. B. (2003). Trafficking of Kv1.4 potassium channels: interdependence of a pore region determinant and a cytoplasmic C-terminal VXXSL determinant in regulating cell-surface trafficking. *Biochem. J.* **375**, 761-768.